Landau level degeneracy and quantum Hall effect in a graphite bilayer

Edward McCann and Vladimir I. Fal'ko
Department of Physics, Lancaster University, Lancaster, LA1 4YB, United Kingdom

We derive an effective two-dimensional Hamiltonian to describe the low energy electronic excitations of a graphite bilayer, which correspond to chiral quasiparticles with a parabolic dispersion exhibiting Berry phase 2π. Its high-magnetic-field Landau level spectrum consists of almost equidistant groups of four-fold degenerate states at finite energy and eight zero-energy states. This can be translated into the Hall conductivity dependence on carrier density, $\sigma_{xy}(N)$, which exhibits plateaus at integer values of $4e^2/h$ and has a "double" $8e^2/h$ step between the hole and electron gases across zero density, in contrast to $(4n+2)e^2/h$ sequencing in a monolayer.

PACS numbers: 73.63.Bd, 71.70.Di, 73.43.Cd, 81.05.Uw

For many decades, the electronic properties of a graphite monolayer have attracted theoretical interest due to a Dirac-type spectrum of charge carriers [1, 2, 3, 4, 5, 6] in this gapless semiconductor [7]. Recently Novoselov *et al.* [8] fabricated ultra-thin graphitic devices including monolayer structures. This was followed by further observations [9, 10, 11] of the classical and quantum Hall effects (QHE) in such systems confirming the expectations [3] of an unusual phase of Shubnikov de Haas oscillations and QHE plateaus sequencing, as manifestations of a peculiar magneto-spectrum of chiral Dirac-type quasiparticles containing a Landau level at zero energy [1].

In this Letter we show that quasiparticles in a graphite bilayer display even more intriguing properties including a peculiar Landau level (LL) spectrum: these are chiral quasiparticles exhibiting Berry phase 2π, with a dominantly parabolic dispersion and a double-degenerate zero-energy LL incorporating two different orbital states with the same energy. Taking into account spin and valley degeneracies, the zero-energy LL in a bilayer is 8-fold degenerate, as compared to the 4-fold degeneracy of other bilayer states and the 4-fold degeneracy of all LLs in a monolayer. The structure and degeneracies of the Landau level spectrum in a bilayer determine a specific sequencing of plateaus in the density dependence of the QHE conductivity $\sigma_{xy}(N)$ which is distinguishably different from that of Dirac-type quasiparticles in a graphite monolayer and of non-chiral carriers in conventional semiconductor structures.

We model a graphite bilayer as two coupled hexagonal lattices including inequivalent sites A, B and $\tilde{A}, \tilde{B}$ in the bottom and top layers, respectively. These are arranged according to Bernal ($\tilde{A}$-B) stacking [7, 12, 13], as shown in Fig. 1. A lattice with such symmetry supports a degeneracy point at each of two inequivalent corners, K and $\tilde{K}$, of the hexagonal Brillouin zone [14], which coincide with the Fermi point in a neutral structure and determine the centers of two valleys of a gapless spectrum. At the degeneracy point, electron states on inequivalent (A/B or $\tilde{A}/\tilde{B}$) sublattices in a single layer are decoupled, whereas interlayer coupling $\gamma_{\tilde{A}B} \equiv \gamma_1$ forms 'dimers' from pairs of $\tilde{A}$-B orbitals in a bilayer [solid circles in Fig. 1], thus

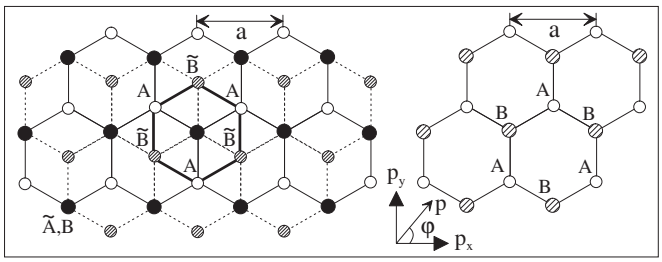

FIG. 1: Left: schematic of the bilayer lattice (bonds in the bottom layer A, B are indicated by solid lines and in the top layer $\tilde{A}, \tilde{B}$ by dashed lines) containing four sites in the unit cell: A (white circles), $\tilde{B}$ (hashed), $\tilde{A}B$ dimer (solid). Right: the lattice of a monolayer.

leading to the formation of high energy bands [12, 13].

The low energy states of electrons are described by

$$\hat{H}_2 = -\frac{1}{2m}\begin{pmatrix} 0 & (\pi^\dagger)^2 \\ \pi^2 & 0 \end{pmatrix} + \hat{h}_w + \hat{h}_a; \qquad (1)$$

$$\hat{h}_w = \xi v_3 \begin{pmatrix} 0 & \pi \\ \pi^\dagger & 0 \end{pmatrix}, \quad \text{where} \quad \pi = p_x + ip_y;$$

$$\hat{h}_a = \xi u \left[\tfrac{1}{2}\begin{pmatrix} 1 & 0 \\ 0 & -1 \end{pmatrix} - \frac{v^2}{\gamma_1^2}\begin{pmatrix} \pi^\dagger\pi & 0 \\ 0 & -\pi\pi^\dagger \end{pmatrix} \right].$$

The effective Hamiltonian $\hat{H}_2$ operates in the space of two-component wave functions Φ describing electronic amplitudes on A and $\tilde{B}$ sites and it is applicable within the energy range $|\varepsilon| < \frac{1}{4}\gamma_1$. In the valley K, $\xi = +1$, we determine $\Phi_{\xi=+1} = (\phi(A), \phi(\tilde{B}))$, whereas in the valley $\tilde{K}$, $\xi = -1$ and the order of components is reversed, $\Phi_{\xi=-1} = (\phi(\tilde{B}), \phi(A))$. Here, we take into account two possible ways of $A \rightleftharpoons \tilde{B}$ hopping: via the dimer state (the main part) or due to a weak direct $A\tilde{B}$ coupling, $\gamma_{A\tilde{B}} \equiv \gamma_3 \ll \gamma_{\tilde{A}B}$ (the term $\hat{h}_w$). They determine the mass $m = \gamma_1/2v^2$ and velocity $v_3 = \left(\sqrt{3}/2\right) a\gamma_{A\tilde{B}}/\hbar$. Other weaker tunneling processes [7] are neglected. The term $\hat{h}_a$ takes into account a possible asymmetry between top and bottom layers (thus opening a mini-gap $\sim u$).

For comparison, the monolayer Hamiltonian [2],

$$\hat{H}_1 = \xi v \begin{pmatrix} 0 & \pi^\dagger \\ \pi & 0 \end{pmatrix} \equiv \xi v \left(\sigma_x p_x + \sigma_y p_y\right),$$

is dominated by nearest neighbor intralayer hopping $\gamma_{AB} = \gamma_{BA} \equiv \gamma_0 \gg \gamma_1$, so that $v = \left(\sqrt{3}/2\right) a\gamma_{AB}/\hbar$. For equivalent parameters in bulk graphite [7], $v_3 \ll v$ in Eq. (1). Thus, the linear term $\hat{h}_w$, which is similar to $\hat{H}_1$, is relevant only for very small electron momenta (i.e., in an electron gas with a small density at a very low magnetic field) whereas the energy spectrum within the interval $\frac{1}{2}\gamma_1(v_3/v)^2 < |\varepsilon| < \frac{1}{4}\gamma_1$ is dominated by the first term [15] in $\hat{H}_2$ producing a dispersion $|\epsilon| = p^2/2m$, which contrasts with $|\epsilon| = vp$ in a monolayer. $\hat{H}_1$ and $\hat{H}_2$ form a family of Hamiltonians $\hat{H}_J = \xi^J f(|p|)\,\sigma\cdot\mathbf{n}$ describing particles which are chiral in the sublattice space, where $\mathbf{n} = \mathbf{l}_x\cos(J\varphi) + \mathbf{l}_y\sin(J\varphi)$ for $\mathbf{p}/p = (\cos\varphi, \sin\varphi)$ [$\pi = pe^{i\varphi}$], and the degree of chirality is $J = 1$ in a monolayer and $J = 2$ in the bilayer. It is interesting to notice that quasiparticles described by the Hamiltonians $\hat{H}_J$ acquire a Berry phase $J\pi$ upon an adiabatic propagation along a closed orbit, thus charge carriers in a bilayer are Berry phase 2π quasiparticles, in contrast to Berry phase π particles in the monolayer of graphene [3]. According to the inverted definition of sublattice components (for which we reserve 2×2 Pauli matrices σ_i [16]) of the wave functions $\Phi_{\xi=+1}$ and $\Phi_{\xi=-1}$, quasiparticles in different valleys, $\xi = \pm 1$ have effectively the opposite chirality. Also, the existence of two valleys is crucial for the time-reversal symmetry of the chiral Hamiltonians. In application to $\hat{H}_2$, time reversal is described by $(\Pi_1 \otimes \sigma_x)\hat{H}^*(\mathbf{p}, B, u)(\Pi_1 \otimes \sigma_x) = \hat{H}(-\mathbf{p}, -B, u)$, where Π_1 swaps $\xi = +1$ and $\xi = -1$ in valley space [16].

A microscopic analysis leading to the bilayer Hamiltonian $\hat{H}_2$ uses the tight-binding model of graphite and the Slonczewski-Weiss-McClure parameterization [7] of relevant couplings. We represent the Hamiltonian near the centers of the valleys in a basis with components corresponding to atomic sites $A, \tilde{B}, \tilde{A}, B$ in the valley K [14] and to $\tilde{B}, A, B, \tilde{A}$ in the valley $\tilde{K}$, and distinguish between on-site energies, $\pm\frac{1}{2}u$ in the two layers,

$$\mathcal{H} = \xi \begin{pmatrix} \frac{1}{2}u & v_3\pi & 0 & v\pi^\dagger \\ v_3\pi^\dagger & -\frac{1}{2}u & v\pi & 0 \\ 0 & v\pi^\dagger & -\frac{1}{2}u & \xi\gamma_1 \\ v\pi & 0 & \xi\gamma_1 & \frac{1}{2}u \end{pmatrix}; \quad \begin{cases} \pi = p_x + ip_y, \\ \mathbf{p} = -i\hbar\nabla - e\mathbf{A}, \\ \mathbf{B} = \mathrm{rot}\mathbf{A}, \\ [\pi, \pi^\dagger] = 2\hbar eB. \end{cases}$$

The Hamiltonian $\mathcal{H}$ determines the following spectrum of electrons in a bilayer at zero magnetic field. There are four valley-degenerate bands, $\epsilon_\alpha^{\pm}(\mathbf{p})$, $\alpha = 1, 2$, with

$$\epsilon_\alpha^2 = \frac{\gamma_1^2}{2} + \frac{u^2}{4} + \left(v^2 + \frac{v_3^2}{2}\right)p^2 + (-1)^\alpha \left[\frac{\left(\gamma_1^2 - v_3^2p^2\right)^2}{4} + v^2p^2\left[\gamma_1^2 + u^2 + v_3^2p^2\right] + 2\xi\gamma_1 v_3 v^2 p^3\cos 3\varphi\right]^{1/2},$$

where ϵ_2 describes the higher-energy ($\tilde{A}B$ dimer) bands.

The dispersion $\epsilon_1(p)$ describes low energy bands. In the intermediate energy range, $\frac{1}{2}\gamma_1\left(v_3/v\right)^2, u < |\epsilon_1| < \gamma_1$, it can be approximated with

$$\epsilon_1^{\pm} \approx \pm\tfrac{1}{2}\gamma_1\left[\sqrt{1 + 4v^2p^2/\gamma_1^2} - 1\right]. \qquad (2)$$

This corresponds to the effective mass for electrons near the Fermi energy in a 2D gas with density N, $m_c = p/(\partial\epsilon_1/\partial p) = \left(\gamma_1/2v^2\right)\sqrt{1 + 4\pi\hbar^2v^2N/\gamma_1^2}$. The relation in Eq. (2) interpolates between a linear spectrum $\epsilon_1 \approx vp$ at high momenta and a quadratic spectrum $\epsilon_1 \approx p^2/2m$, where $m = \gamma_1/2v^2$. Such a crossover happens at $p \approx \gamma_1/2v$, which corresponds to the carrier density $N^* \approx \gamma_1^2/\left(4\pi\hbar^2v^2\right)$. The experimental graphite values [7, 10] give $N^* \approx 4.36\times 10^{12}cm^{-2}$, whereas the dimer band ϵ_2 becomes occupied only if the carrier density exceeds $N^{(2)} \approx 2\gamma_1^2/\left(\pi\hbar^2v^2\right) \approx 8N^* \approx 3.49\times 10^{13}cm^{-2}$. The estimated effective mass m is light: $m \approx 0.054m_e$ using the bulk graphite values [7, 10].

The 4×4 Hamiltonian $\mathcal{H}$ contains information about the higher energy band ϵ_2, and, therefore, is not convenient for the analysis of transport properties of a bilayer which are formed by carriers in the low energy band ϵ_1. We separate $\mathcal{H}$ into 2×2 blocks, where the upper left diagonal block is $H_{11} \equiv \xi(\frac{1}{2}u\sigma_z + v_3[\sigma_x p_x - \sigma_y p_y])$, the lower right diagonal block is $H_{22} = -\frac{1}{2}\xi u\sigma_z + \gamma_1\sigma_x$, and the off-diagonal blocks are $H_{21} = H_{12} = v\xi(\sigma_x p_x + \sigma_y p_y)$. Then, we take the 4×4 Green function determined by $\mathcal{H}$, evaluate the block G_{11} related to the lower-band states, and use it to identify the effective low-energy bilayer Hamiltonian $\hat{H}_2$. Using $G_{\alpha\alpha}^{(0)} = \left(H_{\alpha\alpha} - \varepsilon\right)^{-1}$, we write

$$G = \begin{pmatrix} G_{11} & G_{12} \\ G_{21} & G_{22} \end{pmatrix} = \begin{pmatrix} G_{11}^{(0)-1} & H_{12} \\ H_{21} & G_{22}^{(0)-1} \end{pmatrix}^{-1} \equiv (\mathcal{H} - \varepsilon)^{-1}.$$

Then, we find that $G_{11} = \left(1 - G_{11}^{(0)}H_{12}G_{22}^{(0)}H_{21}\right)^{-1}G_{11}^{(0)}$, so that $G_{11}^{-1} + \varepsilon = H_{11} - H_{12}G_{22}^{(0)}H_{21}$. Since $|\varepsilon| \ll \gamma_1$, we expand $G_{22}^{(0)} = \left(H_{22} - \varepsilon\right)^{-1}$ in γ_1^{-1}, keeping only terms up to quadratic in $\mathbf{p}$ (and therefore in $\pi^\dagger, \pi$), and arrive at the expression in Eq. (1).

For low quasiparticle energies, $|\varepsilon| \ll \gamma_1$, the spectrum determined by $\hat{H}_2$ in Eq. (1) agrees with $\epsilon_1(p)$ found using the 4×4 Hamiltonian $\mathcal{H}$. Similarly to bulk graphite [7, 17], the effect of $\hat{h}_w$ consists of trigonal warping, which deforms the isoenergetic lines along the directions $\varphi = \varphi_0$, as shown in Fig. 2. For the valley K, $\varphi_0 = 0$, $\frac{2}{3}\pi$ and $\frac{4}{3}\pi$, whereas for $\tilde{K}$, $\varphi_0 = \pi$, $\frac{1}{3}\pi$ and $\frac{5}{3}\pi$. At the lowest energies $|\varepsilon| < \frac{1}{2}\gamma_1\left(v_3/v\right)^2$, trigonal warping breaks the isoenergetic line into four pockets, which can be referred to as one "central" and three "leg" parts [17]. The central part and leg parts have minimum $|\varepsilon| = \frac{1}{2}u$ at $p = 0$ and at $|p| = \gamma_1 v_3/v^2$, angle φ_0, respectively. For $v_3 \sim 0.1v$, we find (using the data in Ref. [7]) that the separation of a 2D Fermi line into four pockets would take place for very small carrier densities

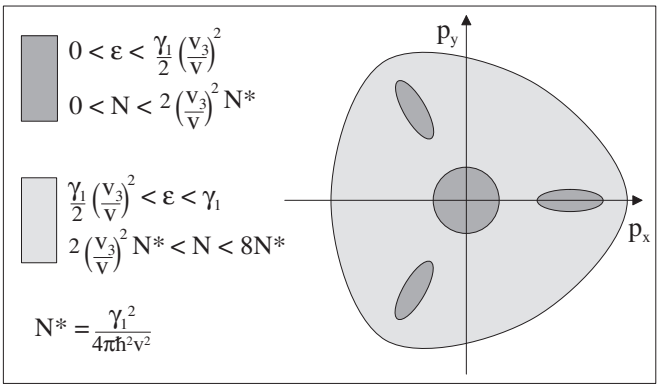

FIG. 2: Schematic of the Fermi line in the valley K, $\xi = 1$, for high (light shading) and low density (dark shading). Note that the asymmetry of the Fermi line at valley $\tilde{K}$, $\xi = -1$, is inverted.

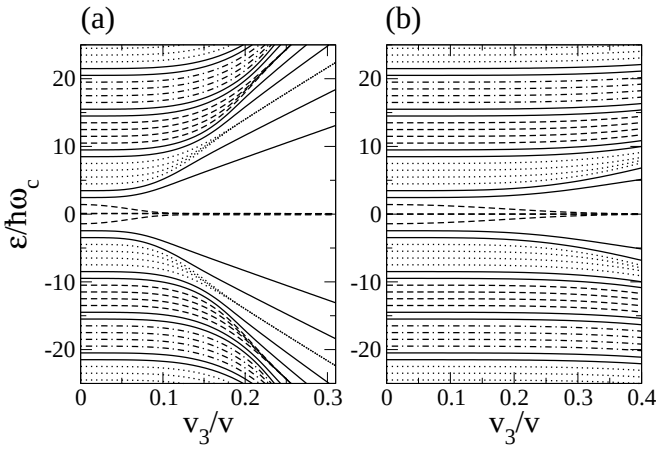

FIG. 3: Numerically calculated Landau levels for various values of v_3 for valley K, $\xi = 1$. (a) for $B = 0.1T$ ($\hbar\omega_c = 0.216meV$ assuming $\gamma_1 = 0.39eV$, $v = 8.0 \times 10^5 m/s$), (b) for $B = 1T$ ($\hbar\omega_c = 2.16meV$). Broken lines show groups of four consecutive levels that become degenerate at large v_3, with each group separated from the next by two solid lines representing levels that are not degenerate.

$N < N_c = 2(v_3/v)^2 N^* \sim 1 \times 10^{11} cm^{-2}$. For $N < N_c$, the central part of the Fermi surface is approximately circular with area $\mathcal{A}_c \approx \pi\varepsilon^2/(\hbar v_3)^2$, and each leg part is elliptical with area $\mathcal{A}_l \approx \frac{1}{3}\mathcal{A}_c$. This determines the following sequencing of the first few LL's in a low magnetic field, $B \ll B_c \approx hN_c/4e \sim 1T$. Every third Landau level from the central part has the same energy as levels from each of the leg pockets, resulting in groups of four degenerate states. These groups of four would be separated by two non-degenerate LLs arising from the central pocket.

In structures with densities $N > N_c$ or for strong magnetic fields $B > B_c$, the above described LL spectrum evolves into an almost equidistant staircase of levels. We derive such a spectrum numerically from Eq. (1) using the Landau gauge $\mathbf{A} = (0, Bx)$, in which operators $\pi^\dagger$ and π coincide with raising and lowering operators [18] in the basis of Landau functions $e^{iky}\phi_n(x)$, such that $\pi^\dagger\phi_n = i(\hbar/\lambda_B)\sqrt{2(n+1)}\phi_{n+1}$, $\pi\,\phi_n = -i(\hbar/\lambda_B)\sqrt{2n}\phi_{n-1}$, and $\pi\,\phi_0 = 0$, where $\lambda_B = \sqrt{\hbar/(eB)}$. In this we followed an approach applied earlier to bulk graphite [17] and used the bulk parameters for intralayer v and interlayer γ_1, varying the value of the least known parameter v_3. The spectrum for the valley K ($\xi = 1$) is shown in Fig. 3 as a function of the ratio v_3/v for two different fields. Fig. 3(a) shows the evolution of the twenty lowest levels for $B = 0.1T$ as a function of v_3, illustrating the above-mentioned crossover from an equidistant ladder at $v_3 = 0$ to groups of pocket-related levels.

The LL spectrum obtained for $B = 1T$, Fig. 3(b) remains independent of v_3 over a broad range of its values. Hence, even in the absence of a definite value of v_3, we are confident that the LL spectrum in bilayers studied over the field range where $\hbar\lambda_B^{-1} > v_3 m$ can be adequately described by neglecting v_3, thus using an approximate Hamiltonian given by the first term in $\hat{H}_2$, Eq. (1). The resulting spectrum contains almost equidistant energy levels which are weakly split in valleys K ($\xi = +1$) and $\tilde{K}$ ($\xi = -1$),

$$\begin{aligned} \varepsilon_n^{\pm} &= \pm\hbar\omega_c\sqrt{n(n-1)} - \tfrac{1}{2}\xi\delta, \ \text{ for } n \geq 2, \\ \Phi_{n\xi} &\equiv C_{n\xi}\left(\phi_n, D_{n\xi}\phi_{n-2}\right), \quad \delta = u\hbar\omega_c/\gamma_1. \end{aligned} \tag{3}$$

Here, $\omega_c = eB/m$, ε_n^+ and ε_n^- are assigned to electron and hole states, respectively, and $D_{n\xi} = [\varepsilon - \xi u/2 + \xi n\delta]/(\hbar\omega_c\sqrt{n(n-1)})$, $C_{n\xi} = 1/\sqrt{1+|D_{n\xi}|^2}$. In the limit of valley ($u = 0$) and spin degeneracies [19], we shall refer to these states as 4-fold degenerate LLs.

The LL spectrum in each valley also contains two levels identified using the fact that $\pi^2\phi_1 = \pi^2\phi_0 = 0$,

$$\begin{cases} \varepsilon_0 = \frac{1}{2}\xi u\,; & \Phi_{0\xi} \equiv (\phi_0, 0); \\ \varepsilon_1 = \frac{1}{2}\xi u - \xi\delta\,; & \Phi_{1\xi} \equiv (\phi_1, 0). \end{cases} \tag{4}$$

According to different definitions of two-component Φ in two valleys, $n = 0, 1$ LL states in the valley K are formed by orbitals predominantly on the A sites from the bottom layer, whereas the corresponding states in the valley $\tilde{K}$ are located on $\tilde{B}$ sites from the top layer, which is reflected by the splitting u between the lowest LL in the two valleys. In a symmetric bilayer ($u = 0$) levels ε_0 and ε_1 are degenerate and have the same energy in valleys K and $\tilde{K}$, thus forming an 8-fold degenerate LL at $\varepsilon = 0$ (here, spin is taken into account). Also, note that the spectrum of high-energy LLs, Eq. (3) is applicable in such fields that $\hbar\lambda_B^{-1} < \gamma_1/2v$. For higher fields the full two-band Hamiltonian $\mathcal{H}$ has to be used to determine the exact LL spectrum, nevertheless, the 8-fold degeneracy of the zero-energy LL remains unchanged.

The group of 8 states at $|\varepsilon| = 0$ (4 for electrons and 4 for holes, Eq.(4)) embedded into the ladder of 4-fold degenerate LL's with $n \geq 2$, Eq. (3) is specific to the magneto-spectrum of $J = 2$ chiral quasiparticles. It

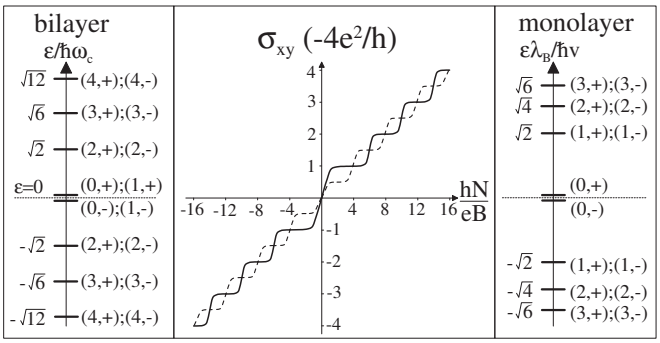

FIG. 4: Landau levels for a bilayer (left) and monolayer (right). Brackets (n,ξ) indicate LL number n and valley index $\xi=\pm1$. In the center the predicted Hall conductivity σ_{xy} (center) as a function of carrier density for bilayer (solid line) is compared to that of a monolayer (dashed line).

would be reflected by the Hall conductivity dependence on carrier density, $\sigma_{xy}(N)$ shown in Fig. 4. A solid line sketches the form of the QHE $\sigma^{(2)}_{xy}(N)$ in a bilayer which exhibits plateaus at integer values of $4e^2/h$ and has a "double" $8e^2/h$ step between the hole and electron gases across $N=0$ that would be accompanied by a maximum in σ_{xx}. Figure 4 is sketched assuming that temperature and the LL broadening hinder small valley and spin splittings as well as the splitting between $n=0,1$ electron/hole LL's in Eqs. (4), so that the percolating states [18] from these levels would not be resolved. To compare, a monolayer has a spectrum containing 4-fold (spin and valley) degenerate LLs [1], $\varepsilon_0=0$ and $\varepsilon^{\pm}_{n\geq1}=\pm\sqrt{2n}\hbar v/\lambda_B$ shown on the r.h.s of Fig. 4, which corresponds to Hall conductivity $\sigma^{(1)}_{xy}(N)$ exhibiting plateaus at $(4n+2)e^2/h$ (dotted line [20]), as discussed in earlier publications [3].

The absence of a $\sigma_{xy}=0$ plateau in the QHE accompanied by the maximum in σ_{xx} in the vicinity of zero density is the result of the existence of the zero-energy LL, which is the fingerprint of a chiral nature of two-dimensional quasiparticles. This contrasts with a gradual freeze-out of both Hall and dissipative conductivities in semicondutor structures upon their depletion. Having compared various types of density dependent Hall conductivity, we suggest that two kinds of chiral (Berry phase $J\pi$) quasiparticles specific to monolayer ($J=1$) and bilayer ($J=2$) systems can be distinguished on the basis of QHE measurements. It is interesting to note that the recent Hall effect study of ultra-thin films by Novoselov *et al.* [10] featured both types of $\sigma_{xy}(N)$ dependence shown in Fig. 4.

It is also worth mentioning that the 8-fold degeneracy of the group of $\epsilon=0$ LLs in a bilayer, Eqs. (4), is quite unusual in 2D systems. It suggests that e-e interaction in a bilayer may give rise to a variety of strongly correlated QHE states. For structures studied in Ref. 10, with electron/hole densities $N\sim10^{12}cm^{-2}$, such a regime may be realized in fields $B\sim10T$.

The authors thank A.Geim, P.Kim, K.Novoselov, and I.Aleiner for useful discussions, and EPSRC for support.

[1] J.W. McClure, Phys. Rev. **104**, 666 (1956).

[2] D. DiVincenzo and E. Mele, Phys. Rev. B **29**, 1685 (1984).

[3] F.D.M. Haldane, Phys. Rev. Lett. **61**, 2015 (1988); Y. Zheng and T. Ando, Phys. Rev. B **65**, 245420 (2002); V. P. Gusynin and S. G. Sharapov, Phys. Rev. Lett. **95**, 146801 (2005); A.H. Castro Neto, F. Guinea, and N. Peres, cond-mat/0509709; N. Peres, F. Guinea, and A.H. Castro Neto, cond-mat/0512091

[4] C. de C. Chamon, C. Mudry, and X.-G. Wen, Phys. Rev. Lett. **77**, 4194 (1996); D.H. Kim, P.A. Lee, X.G. Wen, Phys. Rev. Lett. **79**, 2109 (1997); Y. Hatsugai and P.A. Lee, Phys. Rev. B **48**, 4204 (1993).

[5] D.V. Khveshchenko, Phys. Rev. Lett. **87**, 206401 (2001).

[6] T. Stauber, F. Guinea, and M.A.H. Vozmediano, Phys. Rev. B **71**, 041406 (2005).

[7] M.S. Dresselhaus and G. Dresselhaus, Adv. Phys. **51**, 1 (2002); R.C. Tatar and S. Rabii, Phys. Rev. B **25**, 4126 (1982); J.-C. Charlier, X. Gonze, and J.-P. Michenaud, Phys. Rev. B **43**, 4579 (1991). We quote $\gamma_1=0.39eV$ and $\gamma_3=0.315eV$, neglect the weakest coupling $\gamma_{A\tilde{A}}=\gamma_{B\tilde{B}}\equiv\gamma_4=0.044eV$, and use the experimental values $v=8.0\times10^5m/s$ from Ref. [10]

[8] K.S. Novoselov *et al.*, Science **306**, 666 (2004).

[9] K.S. Novoselov *et al.*, PNAS **102**, 10451 (2005); J.S. Bunch *et al.*, Nano. Lett. **5**, 287 (2005); Y. Zhang *et al.*, Phys. Rev. Lett. **94**, 176803 (2005); C. Berger *et al.*, J. Phys. Chem. B **108**, 19912 (2004).

[10] K.S. Novoselov *et al.*, Nature **438**, 197 (2005).

[11] Y. Zhang *et al.*, Nature **438**, 201 (2005).

[12] S.B. Trickey *et al.*, Phys. Rev. B **45**, 4460 (1992).

[13] K. Yoshizawa, T. Kato, and T. Yamabe, J. Chem. Phys. **105**, 2099 (1996); T. Yumura and K. Yoshizawa, Chem. Phys. **279**, 111 (2002).

[14] Corners of the hexagonal Brilloin zone are $\mathbf{K}_\xi=\xi(\frac{4}{3}\pi a^{-1},0)$, where $\xi=\pm1$ and a is the lattice constant.

[15] $\hat{H}_2\approx-\frac{1}{2m}\left[\sigma_x(p_x^2-p_y^2)+\sigma_y(p_xp_y+p_yp_x)\right]$.

[16] For spatial inversion we use $(\Pi_1\otimes\sigma_0)\hat{H}(\mathbf{p},B,u)(\Pi_1\otimes\sigma_0)=\hat{H}(-\mathbf{p},B,-u)$ where Π_1 swaps $\xi=\pm1$ valleys.

[17] G. Dresselhaus, Phys. Rev. B **10**, 3602 (1974); K. Nakao, J. Phys. Soc. Japan, **40**, 761 (1976); M. Inoue, J. Phys. Soc. Japan, **17**, 808 (1962); O.P. Gupta and P.R. Wallace, Phys. Stat. Sol. B **54**, 53 (1972).

[18] *"The Quantum Hall Effect"*, edited by R.E. Prange and S.M. Girvin (Springer-Verlag, New York, 1986).

[19] Although in graphite the electron g-factor is not small $g=2$, a very light effective mass $m=\gamma_1/2v^2\approx0.054m_e$ in the bilayer determines a small ratio between the Zeeman energy and LL splitting, $\varepsilon_Z/\hbar\omega_c\sim0.05$.

[20] Note that two parallel equivalent monolayers would display Hall conductivity $2\sigma^{(1)}_{xy}(N)$, thus missing every sec-

ond plateau, as compared to $\sigma_{xy}^{(2)}(N)$.